A genetic-based prognostic method for aerospace electromechanical actuators

A GENETIC-BASED PROGNOSTIC METHOD FOR AEROSPACE ELECTROMECHANICAL ACTUATORS

Alessandro Aimasso Pier Carlo Berri Matteo D.L. Dalla Vedova

Department of Mechanics and Aerospace Engineering, Politecnico di Torino

ABSTRACT

Prior awareness of impending failures of primary flight command electromechanical actuators (EMAs) utilizing prognostic algorithms can be extremely useful. Indeed, early detection of the degradation pattern might signal the need to replace the servomechanism before the failure manifests itself. Furthermore, such algorithms frequently use a model-based approach based on a direct comparison of the real (High Fidelity) and monitor (Low Fidelity) systems to discover fault characteristics via optimization methods. The monitor model enables the gathering of accurate and exact data while requiring a minimal amount of processing. This work describes a novel simplified monitor model that accurately reproduces the dynamic response of a typical aerospace EMA. The task of fault detection and identification is carried out by comparing the output signal of the reference system (the high fidelity model) with that acquired from the monitor model. The Genetic Algorithm is then used to optimize the matching between the two signals by iteratively modifying the fault parameters, getting the global minimum of a quadratic error function. Once this is found, the optimization parameters are connected with the assumed progressive failures to assess the system's health. The high-fidelity reference model examined in this study is previously conceptualized, developed, implemented in MATLAB-Simulink and finally experimentally confirmed.

Keywords: actuators, aerospace, safety, Genetic Algorithm, prognostics

1 INTRODUCTION

Primary flight controls represent one of the most critical features in the aircraft system design and, for this reason, they are developed with a conservative safe-life approach. The aforementioned technique consists in replacing associated components after a certain number of flight hours or operating cycle which is previously defined by the normative. However, the employ of this approach does not let us to assess the actual condition of the components, and maintenance is only limited to the specific scheduled operation. More in details, the initial defects – which could arise from the manufacturing process – are not assessed when safe-life approach is used: thus, they can generate a sudden fault, also able to compromise the aircraft safety.

Contact author: A. Aimasso**,** M.D.L. Dalla Vedova

Corso Duca degli Abruzzi 24, 10129, Torino, Italy
alessandro.a420@gmail.com, matteo.dallavedova@polito.it

Indeed, even if a component does not present any unacceptable behaviour, its gradual degradation often leads to a low efficiency condition, and consequently, the whole system functionality results compromised. Moreover, the detection of the cause and the location of a malfunction is not possible when safe-life criterion is applied. However, an accurate identification of the specific failed subcomponent could be effective in reducing maintenance inefficiencies and costs: for example, the substitution of a single subcomponent, and not of the entire system, might be sufficient to restore the system functionality. Recently, new tools with a high grade of robustness to isolate those incipient have been developed. They are thought in order to detect the most common flight control system failure modes before they start affecting the performance of the whole system, in terms of stability, dynamical response, accuracy positioning or stall force. All these methodologies are at the base of a new engineering discipline which is focused on the prediction of when a particular component is no longer able to be fully effective or to achieve the required performance, thus losing its functionality. This discipline is now called Prognostics and Health Management (PHM) [1,2] and its primary purpose is the evaluation of the ongoing state of the system and the estimation of the Remaining Useful Life (RUL) [3]. It is based on the analysis and prediction of all possible failure scenarios, by developing the ability to detect the early signs of aging. If properly assembled and organized, all these information could represent the input to an appropriate failure propagation model. The evaluation of the system's health is generally named as Fault Detection and Identification (FDI) and it consists in identifying and estimating the entity of faults. Considering that PHM strategies are based on the analysis of the system functional parameters – which are acquired in the form of electrical signals – the use of electromechanical systems, and in particular electromechanical actuators (EMA), results advantageous because no further signal conversion is needed and, consequently, no additional sensors are required. More in details, the complexity and multidisciplinary nature of the monitored systems make the FDI task on EMA particularly challenging: indeed, an acceptable level of accuracy is hardly achievable due to the interactions between different failure modes. A wide choice of FDI techniques is nowadays available in the literature: direct comparison of the system response with an appropriate monitoring model [4,5], spectral analysis of system-specific behaviours [6-8], artificial neural networks [9-12], or several combinations of some of these methods [13,14]. Typically, model-based approaches are more computationally expensive and require proper system knowledge but often give more accurate results than data-driven methods. Indeed, data-driven techniques, despite being computationally less costly – but not considering the offline training phase – approach the system as a black box. Thus, in these last cases, all knowledge of the system behaviour is obtained from the row data, requiring large experimental training data set which, unfortunately, are rarely available [15-17]. The failure management could result more effective by applying PHM strategies in aerospace systems, with a lot of benefits: lower operating costs, less maintenance interventions, lower redundancies installed on board aircraft, but also an improvement of the aircraft safety and reliability and simpler logistic. Consequently, maintenance can be scheduled properly with the instantaneous outcome of limited downtime and related costs, so guaranteeing a better management of spare parts warehouses [18]. Finally, it is important to underline that in recent years prognostic concepts have attracted great interest in the scientific and technological world, above all thanks to the variety of applications, resulting the subject of extensive development and dissemination in the scientific literature field.

2 AIMS OF THE STUDY

In the last decade the use of electromechanical actuators for aircraft flight control systems has increased significantly in the aerospace sector [19,20]. However, some problems about their reliability make their use still limited in safety-critical applications [21]: for this reason, PHM covers a crucial role to apply EMAs in the aerospace industry.

So, in this work a new FDI method is proposed: it is based on genetic algorithms (GAs) and it is conceived for EMAs equipped with a permanent magnet sinusoidal motor (PMSM). Moreover, a numerical EMA virtual test bench is designed and modelled to develop and validate this process.

The purpose is to propose an algorithm with a precision which results at least comparable to the existing ones but, at the same time, without requiring large data sets for the automatic learning tools formation, or excessive computational times. More precisely, a computation time of the order of minutes is considered acceptable for detecting slow progressing faults. Then, the proposed technique is tested in different failure condition to evaluate its robustness and field of applicability. According to [13], the FDI algorithm was tested with five different progressive failure modes: partial PMSM coil short circuit, backlash, dry friction, drift of the proportional gain of the PID (Proportional-Integrative-Derivative) position control logic and rotor eccentricity. As reported by [15] they represent the most common damages affecting EMAs and all of them usually have progressive evolution. Besides, otherwise from how available in the literature [7,20,21], the proposed algorithm can address multiple fault modes, also affecting different actuator subsystems simultaneously.

3 EMA ARCHITECTURE

The current trend about the development of new flight control systems is to progressively replace the traditional hydro-mechanical and electro-hydraulic actuators with EMAs, pursuing the “More Electric Aircraft” [22] or the “All Electric Aircraft” [23] concepts. Nowadays, these technologic solutions are already implemented on next-generation aircraft – such as B-787 or A 320 [24,25] – but they are generally relegated to secondary flight control systems and non-safety critical applications [26]. Figure 1 resumes the general EMA architecture: a permanent-magnet sinusoidal motor (PMSM) generates the mechanical power that, thanks to a reduction gearbox, operates the rotational or linear motion of the final user – like flight control surfaces, landing gear or other onboard devices. Moreover, these motors are characterized by a wide range of speed control [27,28]. The magnet and the armature winding are arranged so that the back-electromagnetic force takes a sine wave form; then also the control system shall supply engines with sinusoidal signal [29]. These motors are highly efficient and, if compared to the simpler brushless motors (aka BLDC [30]), they produce less noise, also resulting more resistant to wear: as a result, currently PMSMs are the preferred electric motor type in servomechanism applications (aerospace, automotive, etc.). Finally, a network of sensors (e.g., position, actuation velocity, phase current, temperature) and dedicated actuation control electronic (ACE) close the position control loop. The ACE output lets the Power Electronic to convert the DC or AC electrical supply into the required three-phase power for the PMSM.
The frequency and the amplitude of the motor three-phase sinusoidal currents are regulated as a function of command input and rotor angular position. The application of these systems is relatively recent for the aerospace sector, therefore their reliability and the various failure mode are not yet known and available data does not guarantee a satisfactory confidence level. In addition, some failure modes, potentially compromising the whole system's efficiency, represent a critical issue involving EMA safety. In consequence of these considerations, intense work has been done in recent years to develop robust and effective techniques for prognostics in order to improve the overall safety of operations.

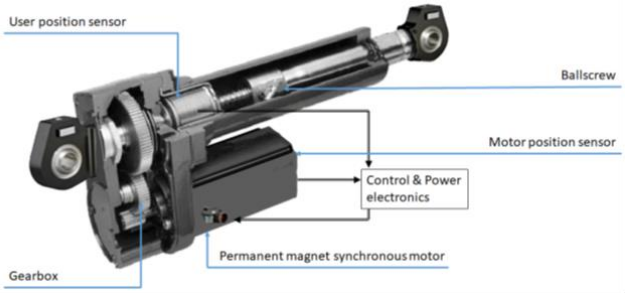

Figure 1. A typical EMA configuration.

4 EMA FAULT MODES

The low EMAs employ in aerospace application makes the cumulated flight hours not enough to provide significant statistics about their most common failure modes. They can be typically summarized into four different failures categories [31]: structural/mechanical, motor, control electronics, sensor. Unfortunately, an electromechanical system could be affected by a failure mode which can’t be faced with prognostic approaches. It is the case of faults types characterized by sudden manifestation and extremely rapid evolution, like breaking of a torsion of the flap transmission. The impossibility of identifying the incipient failure sufficiently in advance limits the typical benefits of the PHM approach. According to [16] this work is focused on five specific progressive failure modes among the most frequent ones in EMAs. More in details, there were considered the effects of mechanical failures resulting from progressive wear, which manifests itself in an increase of backlash and friction; two common PMSM motor failures, the coil-short circuits and the bearing gear generating rotor static eccentricity, together with a drift of the proportional gain of the controller. Indeed, electronic and sensor failures are no less relevant, although their failure precursors are often hard to identify and analyse as they usually occur very quickly, if not instantaneously [27].

5 DEVELOPED MODELS

This research proposes a prognostic tool able to identify early identifying degradation patterns of an EMA, esteeming its actual health status.
To evaluate the robustness and accuracy of this technique, different multi-fidelity model types were developed for the considered mechatronic system.

5.1 HIGH FIDELITY MODEL

The first step of this work is the creation of a High Fidelity, lumped parameters model of an EMA able to collect reference data of the actuator operation, considering different working conditions and the effect of multiple fault modes. It presents a very high level of detail and its general architecture – as reported by the fig 2 – reflects the subsystems and the components hierarchy of common hardware EMAs. More precisely, the model includes:

- The Actuator Control Electronics (ACE) model;
- The Power Electronics Model;
- The Motor Electromagnetic model;
- The Motor and Transmission Dynamical model

It should be noted that this High Fidelity model – despite the reduced dimensionality and its lumped parameter structure – still requires a quite heavy computational effort, so resulting not suitable for iterative evaluations using FDI algorithms. However, it represents the numerical reference model able to simulate the behaviour of a real servomechanism, making possible to early identify the symptoms recognized as the failure precursors of EMA degradations.

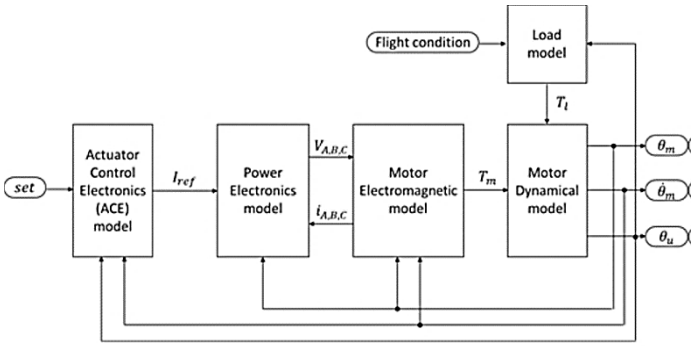

Figure 2. The block diagram of the High Fidelity model.

5.1.1 The Actuator Control Electronic (ACE) model

The Actuator Control Electronics (ACE) model shall determine the torque command to the motor: to obtain this, it implements the control law which compares the commanded position with the feedback signals of measured position and speed.

The control law presents a proportional position loop and a Proportional-Integral-Derivative (PID) velocity loop: more in details, the controller accepts as an input the position or velocity setpoint, the measured motor speed and the measured user position. Using the speed-position mode switch it is possible to choose between a position control mode and a speed control mode; in any case, the velocity setpoint is limited by a saturation accounting for the maximum speed achievable by the motor. Then, a velocity error is fed to a PID controller to determine the required motor torque. Finally, the output of the PID controller has the dimensions of a reference torque for the motor.

5.1.2 The Power Electronic model

The model of Power Electronics determines the motor phase commutation sequence and actuates the current control for each of the motor phases. In this work a Permanent Magnet Synchronous Motor (PMSM) is employed: it is a machine conceptually similar to a BLDC but with a significative different output. Indeed, the stator's polar extension and the permanent magnets on the rotor are arranged to produce a sine wave back-EMF on each of the stator phases. The rotor position is measured using a resolver or an absolute encoder, obtaining a resolution of at least in the order of $1°/P$. In order to produce the maximum torque with minimum current, in usual operating conditions the PMSM power electronics commands a stator current in quadrature with respect to the permanent magnet rotor. In the analysed case, the current setpoint I_{ref} from the control electronics is routed directly to i: this is acceptable if the required performances are compatible with the supply voltage and the nominal back-EMF coefficient of the motor. The current setpoints for the three phases I_{refA}, I_{refB}, I_{refC} are evaluated through inverse Park and inverse Clarke transformations: in order to make this operation, three different reference frames shall be introduced.

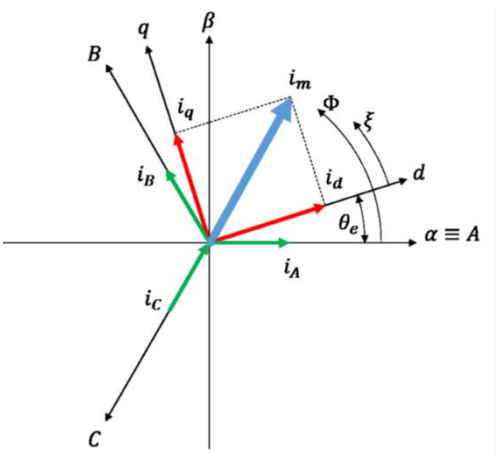

Figure 3. Reference frames for Clark-Park transformations.

- α – β are axes fixed with respect to the stator, the α axis being aligned with the axis of symmetry of the electrical phase A, and the β axis is offset by 90° electrical to form a right-handed frame. The angle Φ is used as a polar coordinate to describe the angles along the stator, starting from the α axis.
- $d - q$ axes are a reference frame rotating with the rotor. The d axis is aligned with a north pole of the rotor, and the q axis is 90° electrical in advance. The angle ξ is used as polar coordinate to describe the angles along the rotor, starting from the d axis.
- The three-phase reference frame with axes A, B, and C aligned with the respective stator phases. The A axis of this reference frame coincides with the α axis.

As reported by the figure, the angle θe is the shift between the $\alpha - \beta$ and the $d - q$ frame. Using two coordinate changes, it is possible to switch between the three reference frames.
More in details, the Clarke transformation allows to convert the current and magnetic flux vectors expressed in the three-phase reference frame to the $\alpha - \beta$ reference frame. Instead, the Park transformation allows to convert the current and magnetic flux vectors from the $\alpha - \beta$ reference frame to the $d - q$ one. Considering the $\alpha - \beta$ reference frame, the current vector is:

$$i = i_\alpha + j i_\beta \tag{1}$$

Instead, in the three-phase reference system *A-B-C*, the current vector is:

$$i = i_A + e^{\frac{j2\pi}{3}} i_B + e^{\frac{j4\pi}{3}} i_C \tag{2}$$

Considering the axes disposition, is then possible to write the following equation for the Park transformation in the matrix form:

$$\begin{bmatrix} i_\alpha \\ i_\beta \end{bmatrix} = \frac{2}{3} \begin{bmatrix} 1 & -\frac{1}{2} & \frac{1}{2} \\ 0 & -\frac{\sqrt{3}}{2} & \frac{\sqrt{3}}{2} \end{bmatrix} \begin{bmatrix} i_A \\ i_B \\ i_C \end{bmatrix} = [B] \begin{bmatrix} i_A \\ i_B \\ i_C \end{bmatrix} \tag{3}$$

Where [B] is the Park matrix.
In the same way, considering the reference frame *d-q* the current vector is:

$$i = i_\alpha + j i_\beta \tag{4}$$

And then in matrix form:

$$\begin{bmatrix} i_d \\ i_q \end{bmatrix} = \begin{bmatrix} \cos(\theta) & sen(\theta) \\ -sen(\theta) & \cos(\theta) \end{bmatrix} \begin{bmatrix} i_\alpha \\ i_\beta \end{bmatrix} = [A] \begin{bmatrix} i_\alpha \\ i_\beta \end{bmatrix} \tag{5}$$

where $[A]$ is the Park matrix.

5.1.3 The Motor Electromagnetic model

The electromagnetic model of the motor computes the torque and the back-EMF produced by the electrical machine. The electromagnetic coupling between rotor and the stator phases is described by three back-EMF coefficients k_a, k_b, k_c. They are defined as the derivative of the magnetic flux concatenated which each phase, with respect to the rotor angle Θ_M. The back-EMF coefficients are calculated considering the distribution of the magnetic field: for the PMSM three sine waves, out of phase by 120°, are computed and multiplied by the nominal back-EMF coefficient. Then, modifying the coefficients

lets to simulate the electrical fault modes. Moreover, a RL circuit is employed to evaluate the phase currents. The circuit is connected with a star arrangement and for each integration timestep the following equations are solved:

$$i_A + i_B + i_C = 0 \quad (6)$$

$$V_j - k_j\omega = R_j i_j + L_j \frac{di_j}{dt} \quad (7)$$

For *j=A,B,C*, while the resistance and inductance of each phase (R_j and L_j) are the nominal values from the motor datasheet.

The currents and the respective back-EMF coefficients are employed to compute the motor torque. Assuming a linear superposition of the contributions of each phase, the total motor torque is calculated as:

$$T_m = \sum_{j=A,B,C} i_j k_j \quad (8)$$

5.1.4 The Motor and Transmission Dynamic model

The model computes the motor and the user positions, receiving as input the motor and external load torques. It is described by the following equation:

$$T_m - T_l = J_m \frac{d^2\theta_m}{dt^2} + C_m \frac{d\theta_m}{dt} \quad (9)$$

Where J_m and C_m are respectively the inertia and the damping of the motor-user assembly. Moreover, the model considers also non-linear phaenomena affecting actuators' behaviour such as friction and backslashes.

5.1.5 The EMA test bench

A specific test bench has been developed to validate the response of the model [32-35,48]. It has got an architecture thought to mirror that of a typical electromechanical actuator for flight controls and it comprehends different components and subsystems. At first, for the actuation section a commercial solution was adopted, in order to reduce costs and time related to the test-bench design and development. Specifically, a PMSM motor were selected – the Siemens 1FK7060-2AC71-1QA0 – which is a permanent magnet, three phase, four pole-pairs driven by a three-phase inverter at 400 V for the power module and by a 24 VDC for the logic section. The inverter controls the phase commutation and it allows to measure currents, voltages and rotor position and speed with a sampling frequency of 400 Hz. The table 1 resumes the most important features of the motor. Then, the test bench employs a compound planetary gearbox as a transmission between the motor and user shaft. The particular architecture proposed for this application guarantees a high gear ratio within a limited size and with few moving parts, so respecting weight and size requirements for aerospace actuation [36]. The gearbox was built through Fused Deposition Modelling (FDM) additive manufacturing, employing a Poly-Lactic Acid polymer. In this way the costs and time associated to manufacturing were limited and the design phase was simplified. The mechanical efficiency was measured at 65%, a satisfying value considering the material employed, while the reverse efficiency is 51%. The output of the gearbox is connected to a high resolution, 5000 pulses per revolution, incremental encoder that allows to close the position control loop. Figure 5.2 (a) shows the general layout of the gearbox while Figure 5.2 (b) the distribution of velocity on the gears, useful to compute the transmission ratio.

Finally, the gearbox is composed by low strength polymeric materials and then it can undergo only a small fraction of the motor stall torque. Then, external loads on the actuator cannot be simulated by applying a torque directly on the output shaft of the gearbox, but a breaking unit is required. The brake is controlled in closed loop to follow a torque setpoint, while an AT328P microcontroller reads the loadcell: this commands a small servomotor to actuate the calliper until the desired torque is applied. At the same time, the microcontroller logs the measured torque to a PC.

Table I - Motor datasheet

Quantity	Unit	Value
Torque gain	Nm/A	1.91
Phase resistance	Ohm	2.75
Phase inductance	mH	30.5
Number of poles	-	8
Max current	A	10.7
Max voltage	V	380
Inertia	$Kgcm^2$	7.7

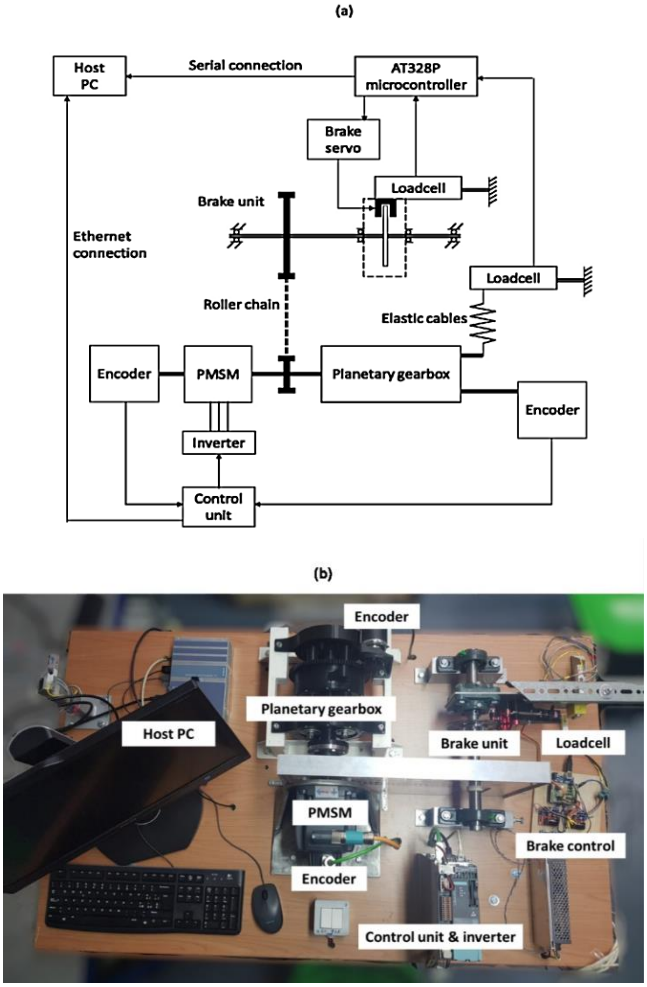

Figure 4. Scheme (a) and photography (b) of the test bench.

5.2 LOW FIDELITY MODEL

To perform the prognostic analysis, a new monitoring model is developed through a simplification of the High Fidelity model already described in chapter 5.1. The most important assumptions introduced to the model's structure are about the electromagnetic subsystem implementation. In this way, the overall complexity and dimensionality result reduced, making the model computationally lighter and faster. More precisely, the three-phases architecture that characterized the PMSM is now replaced by a simplified equivalent single-phase motor [37].

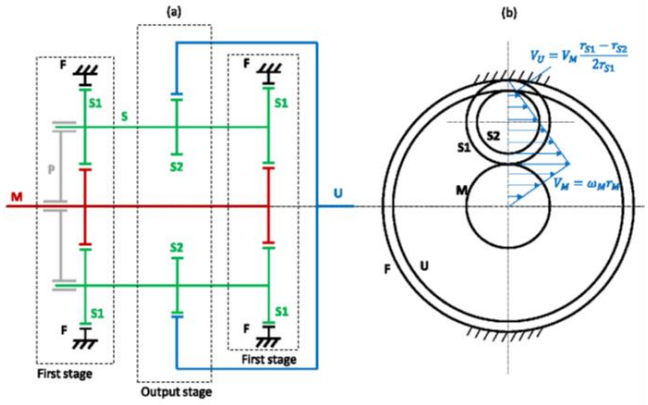

Figure 5. Layout of the compound planetary drive (a) and velocity distribution (b).

It comprehends a more straightforward first-order RL dynamical model based upon equivalent electrical and mechanical characteristics, which are calculated on the base of the actual system's electrical features. Operating as reported by [38], the three-phases motor currents are assumed as a signal to perform the FDI of the real system because it is sensitive to different fault modes. The simplifications implemented bring the LF monitoring model to do not calculate the three-phase current but an equivalent single-phase: consequently, a calibration procedure was developed. This was made by comparing the equivalent single-phase current with the corresponding quadrature current of the PMSM – in turn calculated through the Clarke-Park transformation applied to the three measured currents signals provided by the HF model – knowing that both of them are proportional to the motor's torque. Then, a first-order one degree of freedom non-linear model, with a simplified hysteresis current loop, replaces the complex modelling of PMSM and power electronics implemented in the HF model. Moreover, electrical faults are simulated through a surrogate modelling approach: for this purpose, two shape functions [30] were introduced modulating equivalent stator phase resistance, motor back-EMF coefficient, and torque gain as a function of the rotor angular position. These shape functions do not represent a specific physical phenomenon and they are designed to best approximate the detailed model's behaviour, requiring a lower computational cost. The two shape functions, which describe the eccentricity and short circuit failures affecting the real EMA, are a proper combination of sine waves dependent on failures magnitude, rotor angular position and some calibration factors.
The short circuit (SC) shape function is defined as:

$$\begin{aligned}\varphi_{SC} = k_{FT}\Big\{ & N_A[1 + + k_{FS}\sin^2(\theta_e + \pi)] \\ & + N_B\left[1 + + k_{FS}\sin^2\left(\theta_e + \frac{pi}{3}\right)\right] \\ & + N_C\left[1 + k_{FS}\sin^2\left(\theta_e - \frac{pi}{3}\right)\right]\Big\}\end{aligned} \quad (10)$$

where N_A, N_B, N_C are the fractions of undamaged windings of each phase, k_{FT} and k_{FS} are the global and single contribution calibration coefficients, and ϑ_e is the rotor electrical angular position.
Instead, the shape function of static rotor eccentricity (ECC) [8] is formulated as follows:

$$\varphi_{ECC} = 1 - k_E\zeta\left[\cos(\theta_e + \phi_e\right] \quad (11)$$

where ζ and ϕ_e represent the amplitude and direction of the rotor static eccentricity, respectively, and k_E is an additional eccentricity calibration coefficient. The shape functions coefficients (the global and single contributions of the short circuit calibration coefficients, the eccentricity calibration one, the equivalent torque gain, and the back-EMF coefficient) are initially undefined: then, a calibration process is required.

2.2.2 Model calibration

As already described previously, one of the most important differences between HF and LF models is represented by the architecture of the PMSM motor, with the three-phases architecture replaced by a simplified equivalent single-phase motor. Consequently, a calibration process is required to uniform the output currents of the two models, as shown by the figure. The current is directly proportional to the motor torque and at the first stage of actuation, the signal has initially a linear behaviour. When considering the models in nominal conditions, the currents show comparable trends, but they differ for a small offset in terms of magnitude: this can be regarded as an 'error' and it can be compensated using the Genetic Algorithm included in MATLAB Optimization Toolbox. The error is due to a slightly lower stator-rotor electromagnetic coupling in the monitor model and it causes a higher equivalent current when the same operating conditions (torque and speed) are considered. Hence, a different response can be observed from position and velocity time histories as the faster model will reach first the commanded position. When a fault in the electrical model is taken into account, the angular position phase displacement gives current ripples signal, hindering the correct fault identification. In order to minimize the position error in nominal condition, the coefficient k_e and the motor gain torque GT of the monitor model shall be calibrated by applying the genetic algorithm, in order to minimize the obtained error. The Mean Squared functions is employed to compute the Mean Squared Error (MSE) as follows:

$$MSE = \sum_{i=1}^{n}(I_{HF} - I_{LF})^2 \ [A^2] \quad (12)$$

where I_{HF} and I_{LF} are, respectively, the high fidelity and the low fidelity current components at each integration step, whereas n is the sampling number. Before the calibration, the MSE has a value equal to:

$$MSE_{init} = 0{,}1292\ [A^2] \quad (13)$$

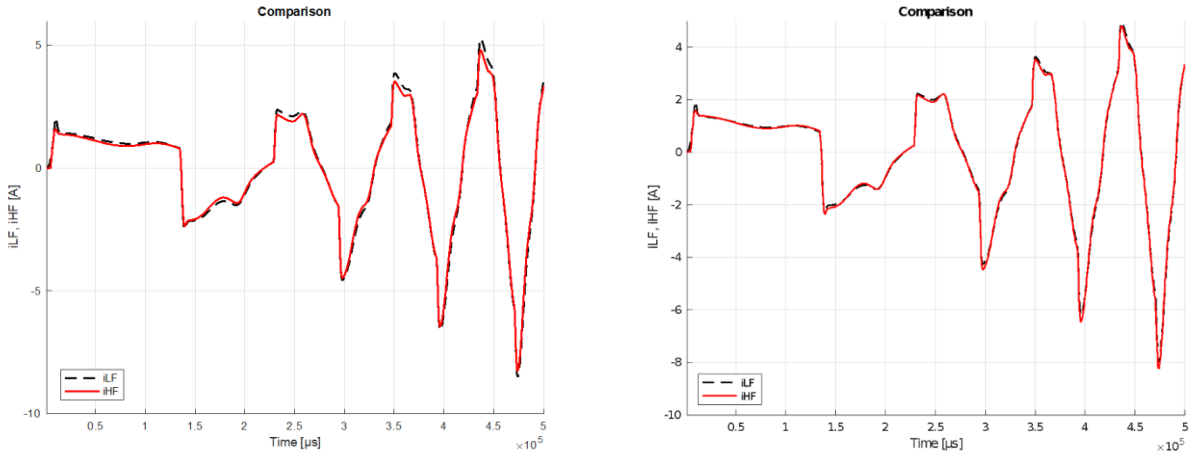

Figure 6. Comparison between the two output currents before (upper) and after (lower) calibration

6 PROPOSED FDI ALGORITHM

Model based FDI is a parameter estimation task [39] which can be solved with an optimization algorithm. An objective function is defined as a cumulative error between the actual system and the model. In this work, the high-fidelity reference model replaces the physical actuator and it is considered as the real model (RM), while the low fidelity model is the monitor model (MM). The optimization updates iteratively a set of parameters encoding the actuator's fault condition and the process is stopped when an adequate match is found between the two responses.

Several optimization techniques can be employed, but as observed in literature [40], most algorithms are more likely to converge to local minima, so failing to find the global solution. This behaviour is harmful to a robust and reliable fault detection, since it can estimate incorrect faults, with a high likelihood of false positives or missed detections. At contrary, more robust global search methods, such as Genetic Algorithms and Simulated Annealing, offer a higher success rate in detecting the global function minimum, at the expense of a longer computational time [38,39].

The core of the proposed FDI strategy is a standard Genetic Algorithm, as available in the MATLAB optimization toolbox [47]. Genetic Algorithms are a class of metaheuristic evolutionary optimization algorithms, inspired by the natural selection process. During each iteration – called generation – the objective function (often referred to as the fitness function) is evaluated in a population of points, called chromosomes or individuals. Each chromosome is a potential solution of the minimization and the individuals of each generation are ranked, according to their fitness. The best ranked individuals are chosen as parents for the next generation: in this way it results composed by the best individuals of the previous iteration and by new ones, which are created using different operators (selection, crossover and mutation).

The process is repeated iteratively until a stopping criterion is satisfied.

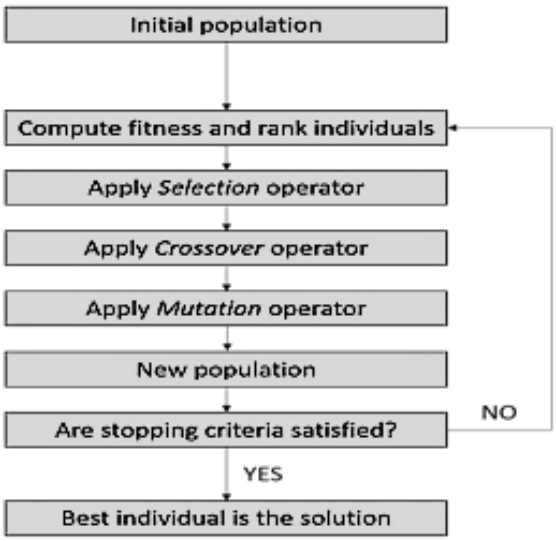

Figure 7. Flow chart of Genetic Algorithm.

Genetic Algorithms (GAs) [41] have been engaged for several applications to solve problems in different fields of application, such as the optimal design of antennas and structural components, the control strategies for robotic applications or the aerodynamic optimization of turbomachinery [42-45]. Generally, they represent the best solution in problems featuring an expensive objective function depending on multiple variables. For this reason, in recent years they have been employed for model-based diagnostic and prognostic tasks, above all for mechatronics applications and electrical machines

According to how previously said, in this work a model-based FDI strategy is developed in order to identify and quantify the faults levels of an EMA. The algorithm analyzes the dynamic response of the system (RM), comparing it with the numerical model (MM) through a GA optimization. Specifically, the analyzed signals are the stator current and the motor speed and the envelope of the three phases is considered to compare the RM three-phase square-wave current with the MM single-phase equivalent current.

More in detail, at each calculation step, the FDI algorithm executes the monitoring model with a certain fault vector k: it contains the values of the faults which are considered during the optimization. Then, an appropriate Fitness Function (FF) is introduced and the *i-th* LF solution is compared with the reference HF one, accordingly updating the elements' values of the fault vector *k*. The Fitness Function (FF) is finally computed with a Modified Total Least Squares Method [30,46], which is tolerant to small phase lags cumulated between the two EMA models, despite the presence of steep gradients and abrupt changes in the equivalent current. The proposed FF is defined as:

$$r = \sum_t \frac{\left(I_1(t_0) - I_2(t_0)\right)^2}{\sqrt{\frac{dI_1(t_0)^2}{dt} + 1}} = \sum_t \frac{\left(I_{HF}(t_0) - I_{LF}(t_0)\right)^2}{\sqrt{\frac{dI_{HF}(t_0)^2}{dt} + 1}} \qquad (14)$$

where I_{HF} is the current of the HF model, I_{LF} is that of LF and t_0 is a generic instant of the simulation.

Once the error function is minimized, the RM and MM responses match at their best. Inasmuch as both models account for the same fault modes and they are validated to show a consistent behaviour over a wide range of operating conditions, the fault parameters of the MM can be considered as an approximation of those initially injected in the RM. A GA is then employed to search the global minimum of the objective function, by varying the fault parameters of the monitor model.

6.1 NORMALIZATION OF THE FAULTS VECTOR

Fault parameters are introduced to both the reference and monitor models in the form of an eight-elements normalized vector k. These elements represent the arguments of the fitness function described in the previous paragraph. Because genetic algorithms are found to provide a faster convergence with normalized parameters, each argument of the fitness function has been made to vary between 0 and 1 by performing a linear interpolation based on the minimum and maximum values for each fault:

- $k(1) \in [0,1]$ refers to the normalized friction fault: $k(1) = 0$ in normal conditions, whereas $k(1) = 1$ when the value is three times the one in normal conditions.
- $k(2) \in [0,1]$ refers to the normalized backlash fault: $k(2) = 0$ in normal conditions, whereas $k(2) = 1$ when the value is one hundred times the one in nominal conditions.
- $k(3), k(4), k(5) \in [0,1]$ represent respectively the normalized short circuit of phases A, B and C: $k(3) = 0$ when phase A is fully functional, whereas $k(3) = 1$ when there's a complete short circuit for the same phase. In order to avoid any divergence through the simulation, whenever two of the three parameters reach simultaneously the maximum value (1), they are immediately set to 0.99 because otherwise two fully short-circuited phases will make the monitor model current diverge to infinite. This condition may lead to the total breakdown of the motor.

- $k(6),\ k(7) \in [0,1]$ represent the eccentricity fault in terms of amplitude and phase. $k(6)$ is the rotor eccentricity amplitude, $k(6) = 0$ when the rotor eccentricity is null whereas $k(6) = 1$ when it is equal to 1. $k(7)$ is the rotor eccentricity phase, which is the direction of the minimum air gap, $k(7) = 0$ when the phase is equal to -π whereas $k(7) = 1$ when it is equal to π. Due to the fact that the eccentricity phase can assume any value between -π and π when the magnitude is null, it can to be suitably managed during the assessment of the function error.
- $k(8) \in [0,1]$ is the proportional gain fault. $k(8) = 0$ when only the 50% of the nominal value is considered and $k(8) = 1$ when the percentage is increased to 150%. Thus, in nominal conditions $k(8) = 0.5$.

Once normalized, the fault vector is:

$$k = [0, 0, 0, 0, 0, 0, 0.5, 0.5]$$

During the execution of the optimization algorithm, the fault parameters of the reference model are varied depending on whether single fault or multiple fault optimization is chosen. By comparing the current trends of the two models, the algorithm generates suitable values of the fault parameters in the monitor model.
The last step of the work is to concretely evaluate fault detection for the considered model. At this step, only a single fault is considered for each optimization process.

6.2 SINGLE FAULT ISOLATION

As previously stated, the reference current is produced by feeding a fault vector *k* into the reference model. The fault detection is then performed by the genetic algorithm which, through the monitor model, attempts to approximate as closely as possible the values of each fault coefficient corresponding to the equivalent current trend. The percentage of error is computed by using the following relation:

$$\%err = 100 \sqrt{\frac{1}{8}\left(\sum_{i=1}^{6}\left(k_i - \bar{k}_i\right)^2 + \bar{k}_6 \cdot \left(k_7 - \bar{k}_7\right)^2 + \left(k_8 - \bar{k}_8\right)^2\right)} \quad (15)$$

where k_i is the value of the *i-th* fault parameter of the monitor model and $\bar{k}_i$ is the corresponding *i-th* fault parameter of the reference model.
The relation 15 is exactly the same as a mean square error with a minor dissimilarity in the definition of the eccentricity phase error k_7, which can assume any value when the eccentricity coefficient ζ is null.
Three distinct objective functions are examined for each fault: the low fault detection (with $\bar{k}_i \leq 0.25$), medium fault detection (with $0.25 < \bar{k}_i < 0.7$) and high fault detection (with $\bar{k}_i \geq 0.7$).
In order to emphasize the stochastic behaviour of the genetic algorithm, ten optimizations have been carried out for each case, with slightly different results being achieved each time.

Table II - Medium friction optimization results

	k_1	k_2	k_3	k_4	k_5	k_6	k_7	k_8	
Ref.	0.5	0	0	0	0	0	0.5	0.5	$\%err$
1	0.4938	0.0102	0.0008	0.0127	0.0079	0.0107	0.7192	0.4858	
	0.62%	1.02%	0.08%	1.27%	0.79%	1.07%	21.92%	1.42%	2.54%
2	0.5012	0.0068	0.0038	0	0.0114	0.0139	0.7530	0.5024	
	0.12%	0.68%	0.38%	0%	1.14%	1.39%	25.30%	0.24%	1.97%
3	0.4841	0.0125	0	0.0084	0	0.0082	0.4084	0.4872	
	1.59%	1.25%	0%	0.84%	0%	0.82%	9.16%	1.28%	2.14%
4	0.4748	0.0183	0.0014	0.0140	0.0036	0	0.6334	0.4775	
	2.52%	1.83%	0.14%	1.4%	0.36%	0%	13.34%	2.25%	3.24%
5	0.4948	0.0179	0.0009	0	0.0006	0.0064	0.3463	0.4933	
	0.52%	1.79%	0.09%	0%	0.06%	0.64%	15.37%	0.67%	2.02%
6	0.4809	0.0033	0	0	0.0032	0.0008	0.1049	0.4768	
	1.91%	0.33%	0%	0%	0.32%	0.08%	39.51%	2.32%	2.37%
7	0.4957	0.0098	0.0034	0.0093	0.0095	0.0021	0.8051	0.4931	
	0.43%	0.98%	0.34%	0.93%	0.95%	0.21%	30.51%	0.69%	1.83%
8	0.4714	0.0046	0	0.0089	0.0014	0.0069	0.9035	0.4873	
	2.86%	0.46%	0%	0.89%	0.14%	0.69%	40.35%	1.27%	1.76%
9	0.4882	0.0075	0.0116	0.0036	0	0.0162	0.0057	0.5036	
	1.18%	0.75%	1.16%	0.36%	0%	1.62%	49.43%	0.36%	2.19%
10	0.5042	0.0221	0.0022	0	0.0093	0	0.5948	0.4904	
	0.42%	2.21%	0.22%	0%	0.93%	0%	9.48%	0.96%	2.59%

Table III - Random multiple fault parameters results

	k_1	k_2	k_3	k_4	k_5	k_6	k_7	k_8	
Ref.	0.2383	0.5003	$5.32\cdot10^{-7}$	0.4503	0.0404	0.0028	0.2785	0.5	***%err***
1	0.2051	0.4727	$9.44\cdot10^{-4}$	0.4414	0.0445	0.0041	0.4334	0.4950	
	3.32%	2.76%	0.09%	0.89%	0.41%	0.13%	15.49%	0.5%	4.46%
2	0.2137	0.4680	0.0111	0.4449	0.0033	0.0006	0.6516	0.4949	
	2.46%	3.23%	1.11%	0.54%	3.71%	0.22%	37.31%	0.51%	5.66%
3	0.2192	0.4858	$5.59\cdot10^{-5}$	0.4421	0.0026	0.0067	0.1195	0.5096	
	1.91%	1.45%	0.01%	0.82%	3.78%	0.39%	15.90%	0.96%	4.67%
4	0.2132	0.4732	0.0015	0.4466	0.0221	0.0010	0.0874	0.4962	
	2.51%	2.71%	0.15%	0.37%	1.83%	0.18%	19.11%	0.38%	4.16%
5	0.2137	0.4813	$2\cdot10^{-4}$	0.4504	0.0021	0.0067	0.1402	0.4970	
	2.46%	1.9%	0.02%	0.01%	3.83%	0.39%	13.83%	0.3%	4.96%
6	0.2143	0.4771	0.0012	0.4545	0.0031	0.0052	0.2438	0.4999	
	2.4%	2.32%	0.12%	0.42%	3.73%	0.24%	3.47%	0.01%	5.03%
7	0.2011	0.4936	$7.9\cdot10^{-4}$	0.5019	0.0178	0.0066	0.5405	0.5350	
	3.72%	0.67%	0.08%	5.16%	2.26%	0.38%	26.20%	3.5%	7.64%
8	0.1959	0.4807	$7.52\cdot10^{-4}$	0.4776	0.0373	0.0017	0.1992	0.4995	
	4.24%	1.96%	0.08%	2.73%	0.31%	0.11%	7.93%	0.05%	5.42%
9	0.2123	0.4780	$2.59\cdot10^{-4}$	0.4660	0.0087	0.0009	0.6436	0.4978	
	2.6%	2.23%	0.03%	1.57%	3.17%	0.19%	36.51%	0.22%	4.93%
10	0.2142	0.4784	$3.5\cdot10^{-5}$	0.4590	0.0018	0.0015	0.9062	0.4996	
	2.41%	2.19%	0%	0.87%	3.86%	0.13%	62.77%	0.04%	5.13%

This process has been applied for different scenarios:

- Friction fault
- Backslash fault
- Short circuit fault
- Rotor Eccentricity fault
- Proportional gain fault

All the aforementioned cases have been assessed by implementing a low (k1=0.25), medium (k1=0.5) and high (k1=0.75) level of damage to analyse the behaviour of the system in each of these scenarios. For each case, ten optimizations have been executed and the results have been reported in the tables below. The table 2 shows the results for the friction fault medium case.

6.2 MULTIPLE FAULTS ISOLATION

In a real scenario, faults do not occur one at a time but there may be situations in which multiple faults are present. In order to test the performance and the accuracy of the genetic algorithm, a multiple fault optimization is executed. The reference values can be introduced either to liking or randomly. The latter method has been chosen and the results acquired are shown in the table 3.

7 CONCLUSIONS

This work enabled the development of a new FDI algorithm for direct comparison of high fidelity and low fidelity models, in order to discover fault characteristics in aerospace EMAs using optimization methods.

The experimental test bench validated the high fidelity model, while the low fidelity produced a very satisfiable approximation thanks to the developed calibration process. Then, it is possible to conclude that the outcomes of this work are consistent with the objectives set.

However, some considerations and future actions could be studied to ulteriorly improve the models' quality.

At first, a critical parameter is represented by the eccentricity phase. Indeed, when it is very low, the FDI process is still limited because it is not phase dependent, and as a result, it may exhibit very high percentual error. But if the eccentricity is very low, the result is not a clear representation of the actual situation, because this error is not significant.

A second task that could improve this process is the analysis of new algorithms that could guarantee better results. Metaheuristic methods, for example, should be investigated, as should hybrid strategies, such as taking into account both genetic and deterministic methods or machine learning techniques.

Finally, it is critical to investigate how the process can be reduced from its current operating time of about 15 minutes to a quasi-real time process. This could be accomplished by intervening on the optimization algorithm and then simplifying the structure of the low fidelity model.

REFERENCES

[1] Byington C S, Watson W, Edwards D and Stoelting P 2004 A Model-Based Approach to Prognostics and Health Management for Flight Control Actuators *Proceedings of the IEEE Aerospace Conference* (Big Sky, MT, USA).

[2] Vachtsevanos G, Lewis F L, Roemer M, Hess A, and Wu B 2008 *Intelligent Fault Diagnosis and Prognosis for Engineering Systems* (John Wiley & Sons).

[3] Berri P C, Dalla Vedova M D L and Mainini L 2021 Computational framework for real-time diagnostics and prognostics of aircraft actuation systems *Computers in Industry* (vol 132 n 103523) https://doi.org/10.1016/j.compind.2021.103523.

[4] Borello L; Dalla Vedova M D L, Jacazio G and Sorli M 2009 A Prognostic Model for Electrohydraulic Servovalves *Proceedings of the Annual Conference of the Prognostics and Health Management Society* (San Diego, CA, USA).

[5] Dalla Vedova M D L, Germanà A, Berri P C and Maggiore P 2019 Model-based fault detection and identification for prognostics of electromechanical actuators using Genetic Algorithms. *Aerospace* (vol 6)

[6] Dalla Vedova M D L, Maggiore P and Pace L 2014 Proposal of Prognostic Parametric Method Applied to an Electrohydraulic Servomechanism Affected by Multiple Failures *WSEAS Transactions on Environment and Development* (vol 10) pp 478–490.

[7] Bindu S and Thomas V V 2018 A Modified Direct-Quadrature Axis Model for Characterization of Air-Gap Mixed Eccentricity Faults in Three-Phase Induction Motor *International Review on Modelling and Simulations (IREMOS)* (vol 11 n 6) p 359.

[8] Belmonte D, Dalla Vedova M D L and Maggiore P 2015 Electromechanical servomechanisms affected by motor static eccentricity: Proposal of fault evaluation algorithm based on spectral analysis techniques *Safety and Reliability of Complex Engineered Systems - Proceedings of the 25th European Safety and Reliability Conference, ESREL 2015* (Zurich) pp 2365–2372.

[9] Battipede M, Dalla Vedova, M D L, Maggiore P and Romeo S 2015 Model based analysis of precursors of electromechanical servomechanisms failures using an artificial neural network *AIAA Modeling and Simulation Technologies Conference* (Kissimmee, FL, USA).

[10] Elasha F, Shanbr S, Li X and Mba D 2019 Prognosis of a Wind Turbine Gearbox Bearing Using Supervised Machine Learning *Sensors* (vol 19 n 3092).

[11] Chen J, Hu W, Cao D, Zhang B, Huang Q, Chen Z and Blaabjerg F 2019 An Imbalance Fault Detection Algorithm for Variable-Speed Wind Turbines: A Deep Learning Approach *Energies* (vol 12 n 2764).

[12] Quattrocchi G, Berri P C, Dalla Vedova, M D L and Maggiore P 2020 Innovative actuator fault identification based on back electromotive force reconstruction *Actuators* (vol 9 n 3) p 50.

[13] Maggiore P, Dalla Vedova M D L, Pace L and Desando A 2015 Evaluation of the correlation coefficient as a prognostic indicator for electromechanical servomechanism failures *International Journal of Prognostics and Health Management* (vol 6 n 1) pp 1–13.

[14] Liu H, Qin C and Liu M 2019 A Rail Fault Diagnosis Method Based on Quartic C2 Hermite Improved Empirical Mode Decomposition Algorithm *Sensors* (vol 19 n 3300).

[15] Balaban E, Bansal P, Stoelting P, Saxena A, Goebel K F and Curran S 2009 A diagnostic approach for electro-mechanical actuators in aerospace systems. *Proceedings of the 2009 IEEE Aerospace Conference* (Big Sky, MT, USA).

[16] Balaban E, Saxena A, Goebel K, Byington C S, Bharadwaj S P and Smith M 2009 Experimental Data Collection and Modeling for Nominal and Fault Conditions on Electro-Mechanical Actuators *Proceedings of the Annual Conference of the Prognostics and Health Management Society* (San Diego, CA).

[17] Balaban E, Saxena A, Narasimhan S, Roychoudhury I, Goebel K and Koopmans M 2010 Airborne Electro-Mechanical Actuator Test Stand for Development of Prognostic Health Management Systems. *Proceedings of the Annual Conference of the Prognostics and Health Management Society* (Portland, OR, USA).

[18] Goebel K, Daigle M, Saxena A, Sankararaman S, Roychoudhury I and Celaya J 2017 *Prognostics: The Science of Making Predictions* (CreateSpace Independent Publishing).

[19] Garcia Garriga A, Govindaraju P, Ponnusamy S S, Cimmino N and Mainini L 2018 A modelling framework to support power architecture trade-off studies for More-Electric Aircraft *Transportation Research Procedia* (vol 29) pp 146-156.

[20] Fico V M, Rodríguez Vázquez A L, Martín Prats M Á and Bernelli-Zazzera F 2019 Failure Detection by Signal Similarity Measurement of Brushless DC Motors *Energies* (vol 12).

[21] De Martin A, Jacazio G and Vachtsevanos G 2017 Windings fault detection and prognosis in electro-mechanical flight control actuators operating in active-active configuration *International Journal of Prognostics and Health Management* (vol 8 n 2).

[22] Quigley R E J 1993 More electric aircraft Proceedings of the Eighth Annual IEEE Applied Power Electronics Conference - APEC 93 (San Diego, CA, USA).

[23] Howse M 2003 All-electric aircraft *Power Engineering* (vol 17) pp 35–37.

[24] Thalin P, Rajamani R and Maré J C 2018 *Fundamentals of Electric Aircraft* (SAE International).

[25] Maré J C 2018 Aerospace Actuators 2: Signal-by-Wire and Power-by-Wire (Wiley & Sons).

[26] Pozzuto G, De Martin A, Pispola G, Palmieri M and Gallorin M 2019 Electrical Flight Control for Load Control and Alleviation System *More Electric Aircraft* (Tolouse, France).

[27] Bernatt J, Glinka T, Jakubiec M, Krol E and Rossa R 2007 Electric motors with permanent magnets with two-zone rotational speed control *Electrical Machines and Power Electronics.*

[28] Jarzebowicz L 2014 Indirect Measurement of Motor Current Derivatives in PMSM Sensorless Drives *Elektronika ir Elektrotechnika* (n 5) pp 23–26

[29] Rudnicki T, Czerwinski R and Sikora 2015 A Examination of permanent magnet motor with sinusoidal back-EMF *IFAC-PapersOnLine* (vol 48 n 4) pp 170–173.

[30] Berri P C, Dalla Vedova M D L and Maggiore P 2016 A Smart Electromechanical Actuator Monitor for New Model-Based Prognostic Algorithms *International Journal of Mechanics and Control* (vol 17 n 2) pp 19–25.

[31] Gökdere L U, Chiu S L, Keller K J and Vian J 2005 Lifetime control of electromechanical actuators Proceedings of the IEEE Aerospace Conference Proceedings (Big Sky, MT, USA).

[32] Boschetti V 2020 *Master's Thesis* Politecnico di Torino (Torino, Italy).

[33] Sciandra P 2020 *Master's Thesis* Politecnico di Torino (Torino, Italy).

[34] Boggio L 2021 *Master's Thesis* Politecnico di Torino (Torino, Italy).

[35] Berri P.C., *PhD's Thesis*, Politecnico di Torino (Torino, Italy).

[36] P. C. Berri, M. D. L. Dalla Vedova, P. Maggiore and G. Riva, "Design and Development of a Planetary Gearbox for Electromechanical Actuator Test Bench through Additive Manufacturing," *Actuators*, vol. 9, no. 2, p. 35, 2020.

[37] Berri P C, Dalla Vedova M D L, Maggiore P and Viglione F 2019 A simplified monitoring model for PMSM servoactuator prognostics *MATEC Web of Conference*

[38] Berri P C, Dalla Vedova M D L and Maggiore P 2018 A simplified monitor model for EMA prognostics *MATEC Web of Conferences* (vol 233 n 00016).

[39] Berri, P.C.; Dalla Vedova, M.D.L.; Mainini, L. Diagnostics of Actuation System Faults from Dynamic Data. In Proceedings of the 6th European Conference on Computational Mechanics (ECCM 6), *European Community on Computational Methods in Applied Sciences* (ECCOMAS), Glasgow, UK, 11–15 June 2018.

[40] Dalla Vedova, M.D.L.; Maggiore, P.; Pace, L. Proposal of Prognostic Parametric Method Applied to an Electrohydraulic Servomechanism Affected by Multiple Failures. *WSEAS Transactions on Environment and Developmen,* 2014, 10, 478–490.

[41] Mitchell, M. *An Introduction to Genetic Algorithms*; MIT Press: Cambridge, UK, 1996.

[42] Mishra, R.G.; Mishra, R.; Kuchhal, P.; Kumari, P. Optimization and Analysis of High Gain Wideband Microstrip Patch Antenna using Genetic Algorithm. *Int. J. Eng. Technol.* 2018, *7*, 176–179.

[43] Kahraman, M.; Erbatur, F. A GA Approach for Simultaneous Structural Optimization. In Proceedings of the International Conference on Structural Engineering, Mechanics and Computation, Cape Town, South Africa, 2–4 April 2001.

[44] Vijay, M.; Jena, D. GA Based Adaptive Controller for 2DOF Robot Manipulator. *IFAC Proc. Vol.* 2016, *47*.

[45] Shimoyama, K.; Yoshimizu, S.; Jeong, S.; Obayashi, S.; Yokono, Y. Multi-Objective Design Optimization for a Steam Turbine Stator Blade Using LES and GA. *J. Comput. Sci. Technol.* 2011, *5*, 134–147.

[46] Markovsky I and S Van Huffel 2007 Overview of total least-squares methods Journal of Signal Processing (vol 10) pp 2283–2302.

[47] Dalla Vedova M.D.L., Germanà A., Berri P.C., Maggiore P., Model-Based Fault Detection and Identification for Prognostics of Electromechanical Actuators Using Genetic Algorithms.

[48] Berri P.C., Dalla Vedova M.D.L., Maggiore P., Design and development of an Electromechanical Actuator test bench for validation of health monitoring models, *ESREL 2021.*